Mode II fatigue delamination growth characterization of a carbon/epoxy laminate at high frequency under vibration loading

Iréne Maillet [a,1], Laurent Michel [b,*], Frédéric Souric [a], Yves Gourinat [b]

[a] DGA Aeronautical Systems, 47 rue St Jean, BP 93123, 31131 Balma, France
[b] Université de Toulouse, CNRS, ISAE-SUPAERO, Institut Clément Ader (ICA), 3 rue Caroline Aigle, 31077 Toulouse cedex 4, France

A B S T R A C T

A fatigue crack propagation test under mode II has been set up for unidirectional composite laminate characterization at high frequency. The specimen is clamped on a shaker and loaded on its first bending resonance mode. This dynamical test allows an accurate delam ination extension monitoring based on the resonance frequency shift. Dynamical tests are conducted at 260 Hz and 400 Hz and their results are compared to those obtained with 10 Hz 3 ENF tests. Fatigue crack propagation results are presented taking into considera tion the loading ratio difference between both test configurations. All results are collapsed in a unique propagation rate curve.

Keywords:
Fiber reinforced polymer matrix
Delamination fatigue
Mode II loading
Frequency effect
Vibratory fatigue

1. Introduction

During their service life aeronautical structures are submitted to vibrations due to turbulent aerodynamic flow. These fluid structure interactions induce not only sonic acoustic fatigue spectra with low amplitude loads at high frequency range but also buffeting or flutter type fatigue with high loads at lower frequency range [1,2]. At high frequency a very high num ber of cycles can be reached. Today certification of composite structures under damage tolerance is generally based on the concept of no growth damage [3]. So whatever the load level and the frequency range, it must be proved that no delamina tion defect propagates under vibration loading. This raises the questions of frequency effects on crack propagation and of methods enabling the investigation of crack propagation under very high cycle fatigue (VHCF).

Delamination will propagate under one of the three following pure modes or a combination of them: the opening mode (Mode I), the sliding mode (Mode II) and the tearing mode (Mode III). Tests for pure mode I and II are largely used to characterize composite material under fatigue loading [4 6]. For the most critical mode, mode I, ASTM has defined the Double Cantilever Beam (DCB) test as a standard [7]. Currently no standard has been officially released for mode II fatigue test. Several test configurations can be used for mode II: the three point bending end notch flexure (ENF), the four point bending end notch flexure (4ENF) and the end loaded split (ELS) [8]. Mode II fatigue tests on fiber reinforced polymers (FRP) are commonly carried out at a frequency up to 10 Hz, under controlled loading ratio and with a test stop criterion related to spec imen compliance. Fatigue behavior of carbon/epoxy laminate in pure mode II up to 10^6 cycles has been widely studied

* Corresponding author. Tel.: +33 (0) 561339141.
E-mail addresses: irene.maillet@intradef.gouv.fr (I. Maillet), laurent.michel@isae.fr (L. Michel).
[1] Principal corresponding author. Tel.: +33 (0) 562575544.

http://dx.doi.org/10.1016/j.engfracmech.2015.08.030

Nomenclature

ΔG	G_{max} G_{min}
ΔG_{eq}	equivalent delta G
$\frac{da}{dN}$	crack propagation rate
γ	Hojo formula material constant
ν_{lt}	Poisson ratio
ν_{tt}	transverse Poisson ratio
ρ	density
φ	phase between input acceleration and specimen displacement
a	current delamination length
a_0	initial delamination length
a_i	specimen delamination size
b	specimen width
C	compliance
C_0	compliance law parameter
d_{imp}	imposed displacement
$dep_{numerical}$	numerical model displacement
$dep_{specimen}$	specimen test displacement
E_f	flexural Young modulus
$E_{numerical}$	numerical model bending modulus
$E_{specimen}$	fitted specimen bending modulus
E_t	transversal Young modulus
ERR	energy release rate
f_f	final frequency of the specimen
$f_{numerical}$	numerical model frequency
f_{sweep}	specimen resonance frequency obtained by frequency sweep
G	ERR
G_c	critical ERR
G_{final}	dynamical test ERR
G_{lt}	shear modulus
G_{max}	maximum ERR
$G_{numerical}$	numerical model ERR
K	stress intensity factor
k	Paris law parameter
k_D	ΔG_{eq} Paris law parameter
L	distance between ENF rollers
L_0	free specimen length
L_e	specimen length
m	compliance law parameter
m	G N curve parameter
m_D	ΔG_{eq} N curve parameter
N	number of cycle
n	Paris law parameter
N_c	critical number of cycles
n_D	ΔG_{eq} Paris law parameter
P	load
p	G N curve parameter
p_D	ΔG_{eq} N curve parameter
R	fatigue loading rate

[9,4,6,10 12]. At this frequency of 10 Hz, more than 11 days are needed to reach 10^6 cycles. In these conditions the exploration of high cycle fatigue (10^6 10^9) is greatly time consuming. One solution to reduce the test time is to increase the test frequency. However, this question doesn't seem to be addressed in the literature for delamination propagation under mode II.

Frequency effects on fatigue life have been widely investigated in the literature on polymers and composite materials [13 15]. For composites most of these studies concern fatigue tests performed at a rather low frequency range from 0.01 Hz to 30 Hz on tension/compression specimens [16,14,17 19]. They show a large dependence of the fatigue behavior of FRP on loading frequency. This is due to the inherent viscoelasticity of organic matrix. Indeed there are two notable frequency effects which oppose each other: creep and hysteretic heating [15]. At low frequencies, creep behavior is predominant

and it reduces fatigue resistance with a decrease in frequency. At higher frequencies, hysteretic behavior leads to a self heating which may turn into a thermal failure and result in a reduction of fatigue life of the component.

Very significant temperature rises have been monitored for the highest frequency tests (10 30 Hz). Xiao [14] studied angle ply APC2 laminates and computed a temperature increase of up to 135 °C. Barron [17] also reported temperature rises up to 90 °C for a carbon fiber/epoxy composite at 20 Hz. This is particularly true for highly hysteretic or viscoelastic materials at the test temperature and also for disoriented lay ups towards the loading direction [17,14,19]. Rotem [20] tested a quasi isotropic graphite/epoxy laminate under reverse loading. He observed that between 2.8 Hz and 10 Hz, when the frequency increases, the heat generation increases too. High temperatures lead to earlier crack initiation in fatigue. Temperature increase due to self heating might also be used to monitor the fatigue life of laminated composites [19]. However it is also reported that at low stress levels this self heating is reduced and disables any thermal failure. Indeed stress level is one of the key factors [13,18,19] for frequency effects.

Some experimentations at much higher frequencies were already achieved in order to accelerate fatigue tests and to reach a very large number of cycles [21 23]. For a frequency of 100 Hz, several authors [21,23] reported limited effects on fatigue life of composite laminates. Wang et al. [22] have even developed an experiment at 20 kHz to perform fatigue tests on epoxy bonded joints. These experiments were possible because specific specimen dimensions and the limited strain amplitudes have restricted any inconvenient self heating effects.

Similarly the geometry of notched specimen used for crack propagation is likely to reduce self heating which is largely dependent upon the capacity of samples to dissipate heat. It is related to the thermal transfer characteristics of the material, to extension of the heated zone and to the specimen surface area to volume ratio [13]. Indeed for notched specimen, the zone of high stresses is localized and the rest of the specimen is able to dissipate enough heat. This limits any large temper ature rise and any thermal failure.

Frequency effects on fatigue crack propagation in polymers are largely dependent upon the polymer itself [13,24 26]. Yuen et al. [25] reported no effect of frequency at room temperature for the PMMA. Merah et al. [26] achieved tests on Chlorinated PolyVinyl Chloride (CPVC) to find the influence of temperature and frequency between 0.1 Hz and 10 Hz. The frequency sensitivity increases with an increase of the fixed test temperature. It is linked by the authors to a major crazing fatigue mechanism. In a study performed on several polymers, Ramsteiner [24] displayed $da/dN \quad f(\triangle K)$ curves for 1 and 10 Hz which are almost identical. However the author reported that crack propagation is faster at 10 Hz than at 1 Hz. It is difficult to get a clear comprehension of frequency effects from these studies.

There are very few studies concerning frequency effects on crack propagation in composites. Nakai et al. [10] performed fatigue crack propagation tests on CF/epoxy laminates at different frequencies and environment. The authors reported an effect of cycle dependance for mode I test and of time dependance for mode II test. Studies on temperature effects are more common. For example Sjorgen et al. [27] investigated the temperature effect on the delamination growth of carbon/epoxy composite in mode II. Fatigue propagation rates at 100 °C at same energy release rate (ERR) are faster than at room temper ature and a decrease of 30% of the critical value is observed in static loading.

In the field of composite delamination propagation, researchers limited their investigation to frequencies lower than or equal to 10 Hz. So the first aim of this work is to develop a simple test approach to perform fatigue crack propagation (FCP) under mode II at higher frequencies. As performed before for mode I [28], fatigue test of cracked specimens is performed under vibration loading at resonance. An ELS type test specimen is loaded to its first bending resonance mode. The loading ratio is then $R \quad 1$. When delamination propagates, resonance frequency decreases [29]. So the resonance frequency is used to monitor the crack propagation. Dynamic tests are achieved for two frequencies 260 Hz and 400 Hz. Results of these tests are compared with more classical ones which are performed with the ENF (End Notched Flexure) configuration on a servo hydraulic machine at 10 Hz and $R \quad 0.1$. Effects of frequency on the behavior of a carbon fiber/epoxy composite are then investigated and discussed together with the possibility to accelerate FCP tests.

2. Material and specimens

The material used in this study was the Hexply® M21 resin and T700 Carbon fiber unidirectional prepreg supplied by Hexcel©. Beam specimens of $180 \times 25 \times 5$ mm^3 were cut out from unidirectional $[0_{10}]_{sym}$ plates cured in a thermal press. The curing procedure followed a standard cycle with a homogenization stage at 150 °C and a curing one at 180 °C as recom mended by the supplier. A 25 μm thickness Teflon film was inserted at mid plane of laminates during stacking operations to create an artificial starter crack (Fig. 1). All specimens were then pre cracked to get at least a 2 mm crack extension before fatigue tests. Mechanical properties of the material were also measured and main results are listed in Table 1.

3. Low frequency fatigue tests

3.1. Test configuration

Low frequency fatigue tests have been performed with an ENF configuration on a servo hydraulic fatigue machine with a 5 kN load cell capacity, at a controlled displacement ratio of $R \quad 0.1$ and at a frequency of 10 Hz. The dimensions of the ENF test device used in this study are given in Fig. 2. All specimens had an initial crack length (a_0) of 15 mm before pre cracking.

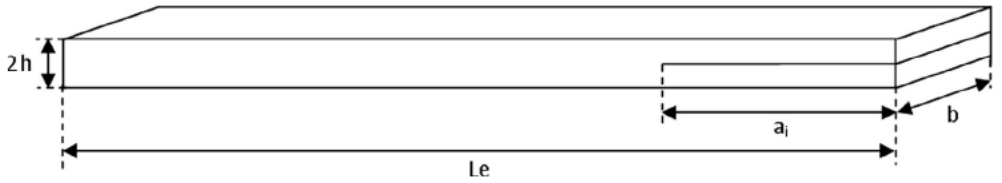

Fig. 1. Specimen geometry.

Table 1
Mechanical properties of the material.

Flexural Young's modulus (E_f)	99.6 GPa
Transversal Young's modulus (E_t)	7.7 GPa
Shear modulus (G_{lt})	4.45 GPa
Poisson's ratio (ν_{lt})	0.33
Transverse Poisson ratio (ν_{tt})	0.4
Density (ρ)	1540 kg/m^3
Critical Energy Restitution Rate in mode II (G_{IIc})	1243 N/m

During fatigue cycling history (Fig. 3 left) arrests were regularly scheduled to measure the crack length in a stereomicro scope with the help of a 1 mm spaced white grid lines painted on the specimen edge (Fig. 3 right). Temperature of the spec imen was also monitored during tests by a thermocouple bonded on specimen surface above the crack tip. The measured increase in temperature has never exceeded +3 °C for all tests. The load was also recorded all along the tests.

3.2. Test procedure

Fig. 4 presents the critical load vs displacement curve issued from a static Mode II ENF study of the T700/M21 material. Experimental results are reported for different initial crack lengths. These results fit very well the curve derived from the compliance law and plotted for the identified value: G_{IIc} 1243 J/m^2.

This curve was used as a guide to fix the maximum imposed displacement of fatigue tests in order to get a stable prop agation all along the test. Within the designed crack length range [15 40 mm] all tests were performed under displacement control. Thus the crack growth rate increased until around 30 mm crack length, in accordance with the maximum energy release rate (ERR) evolution as illustrated in Fig. 4, then it decreased. Specimens used for high speed values, that is at high maximal ERR, were tested at a unique maximum displacement. On the contrary specimens at lower maximal ERR were tested for different maximum displacements in order to extend the investigated ERR's range at low delamination growth rate. Thus only four specimens were used to identify the relation between Crack Propagation Rate $\left(\frac{da}{dN}\right)$ and ERR.

3.3. Data reduction and results

The energy release rate (G) was calculated by the compliance method:

$$G \quad \frac{P^2}{2b}\frac{dC}{da} \tag{1}$$

where P is the load, C the compliance, a the measured crack length and b the specimen width. The evolution of compliance during the fatigue crack propagation was found to follow the static compliance law (Fig. 5) identified beforehand [28].

$$C \quad m \cdot a^3 + C_0 \tag{2}$$

where C_0 and m are parameters of the law.

In Fig. 6, the evolution of crack propagation rate is plotted as a function of the maximum ERR (G_{max}). The fatigue crack propagation curves of the different specimens clearly show that the delamination propagation rate follows a power law rela tionship of the maximum imposed ERR complying with the typical Paris law (Eq. (3)).

$$\frac{da}{dN} \quad k \cdot G_{max}^n \tag{3}$$

where N is the number of cycles, n and k are material constants.

As different successive loadings and different delamination lengths lead to the same Paris law for this material, it is very likely that there is no influence of the loading history or propagation history. Thus as already performed for mode I [28], it is possible to extrapolate a G N onset propagation curve from these results. This curve presents the maximum imposed ERR as

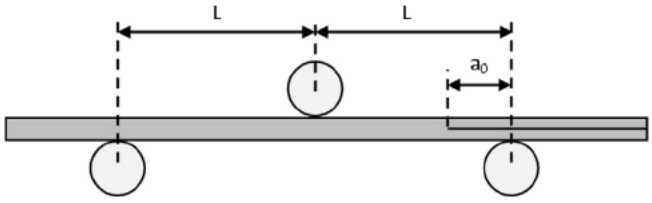

Fig. 2. Schematic ENF test configuration and dimensions: L 50 mm, a_0 15 mm.

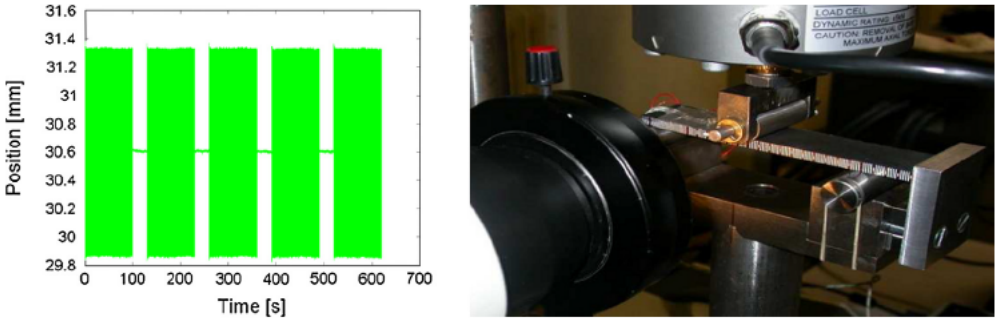

Fig. 3. Crack length measurement: scheduled arrests during cycling (left) and painted grid on specimen edge (right).

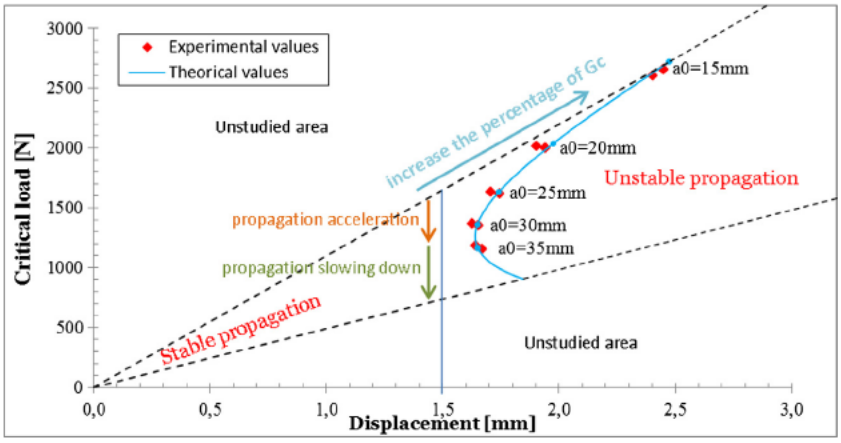

Fig. 4. Critical load–displacement curve of ENF tests for T700/M21 material.

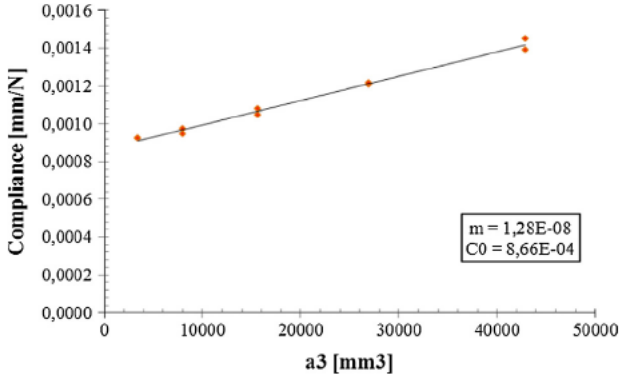

Fig. 5. Static compliance law.

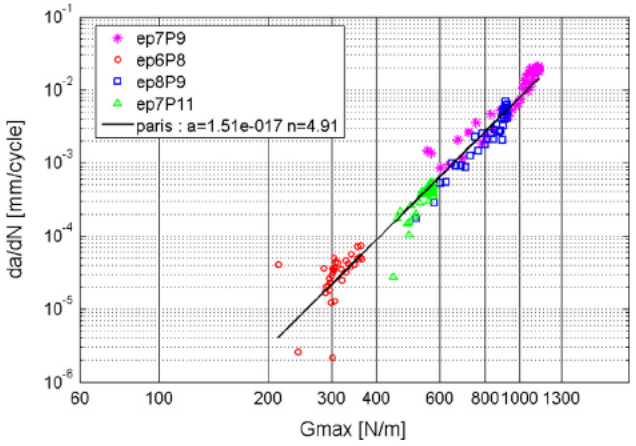

Fig. 6. Propagation rate curve at 10 Hz and R 0.1.

a function of the number of cycles to the propagation onset and offers another interesting way to display delamination growth onset behavior of the material.

The total fatigue crack propagation is divided into segments, each one linked to a propagation threshold. This requires several steps which are illustrated in Fig. 7. The number of cycles used to determine the ERR threshold value is defined as the number of cycles necessary to get a propagation of 0.5 mm of the crack. This increment of length is consistent with the resolution of crack monitoring during our fatigue tests. The total length of propagation is thus divided into segments of 0.5 mm (Fig. 7a). For each first point of segments, the ERR is calculated with the compliance method (Eq. (1)). Then the num ber of cycles needed to propagate the delamination from the first point to the last point of the segment is determined (Fig. 7b). These data are combined to produce a semi log plot of the maximum ERR at propagation onset, G_{max}, vs the critical number of cycles, N_c, as shown in Fig. 7c. The fatigue crack propagation curve is fully used until a maximal delamination size of 40 mm is reached. Indeed at this crack length, results might be inconsistent due to interferences with the pressure cone created by the central roller loading.

Fatigue crack propagation curves of all specimens were analyzed and the resulting global G N onset curve is reported in a semi log plot (Fig. 8). The ERR at propagation onset, G_{max}, takes the form of a power function of the critical number of cycles N_c:

$$G_{max} \quad p \cdot N_c^m \tag{4}$$

where p and m are material constants.

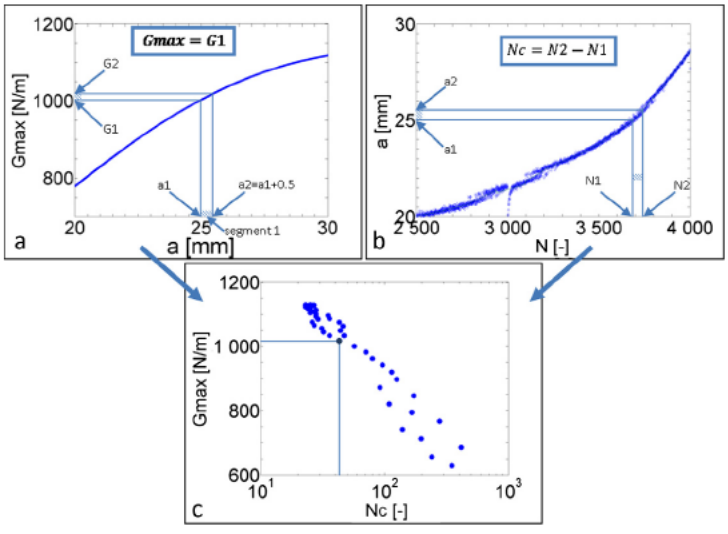

Fig. 7. Extraction of G–N onset curve from fatigue crack propagation curves.

4. High frequency fatigue tests

4.1. Test configuration

High frequency delamination fatigue tests are based on the classical End Loaded Split test configuration [8] under vibra tion loading at resonance. As for ELS configuration, the test sample is fully clamped by its uncracked extremity to a massive rig. But in this case the rig is secured onto an electrodynamic shaker (characteristic: F_{max} 40 kN in sine wave) as shown in Fig. 9. Global acceleration imposed by the shaker serves as the driving force for crack propagation whereas it is a concen trated force which is imposed at the cracked sample extremity for the classical ELS configuration. During the whole, the test specimen is forced to vibrate at its first bending modal frequency in order to take advantage of the large amplification factor of resonance. By changing the free length of the clamped beam (Fig. 10) it is thus possible to perform fatigue crack propa gation tests at very different natural frequencies. Crack propagation will also induce an increase of compliance which will modify the natural resonance frequency of the specimen. This frequency change will be used to monitor the crack extension as detailed in the next section.

The displacement of the specimen was monitored by a laser doppler vibrometer at a point placed at a convenient distance from the clamped end. This allows to get a sensitive measure of the beam displacement within a limited scale. The tests were performed under displacement control at two resonance frequencies (260 Hz and 400 Hz) and with a displacement ratio of R 1.

The temperature evolution of specimens was recorded by a mid wavelength thermal infrared camera (sensitivity between 3 and 5 μm) (Fig. 9) in order to accurately monitor any self heating due to the vibration loading. Data collection has been processed by selecting a limited area around the crack front and by monitoring the time evolution of the hot point

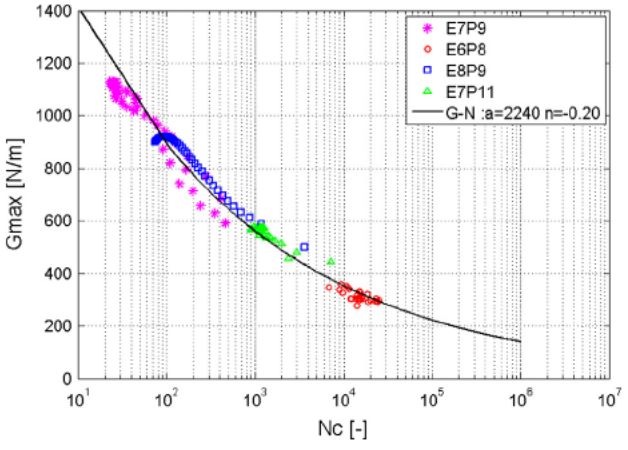

Fig. 8. *G–N* onset propagation curve at 10 Hz and R 0.1.

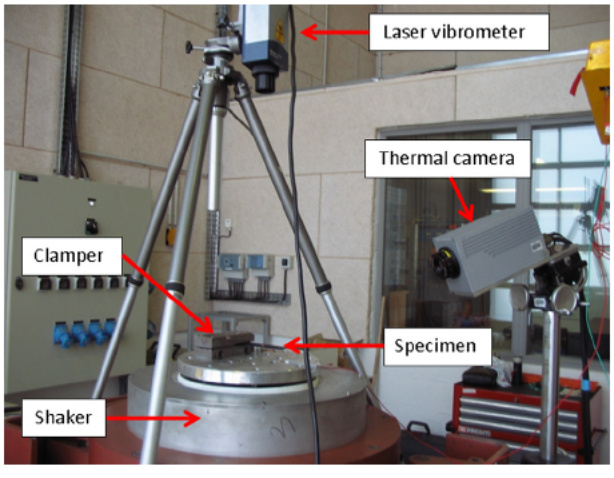

Fig. 9. Test device.

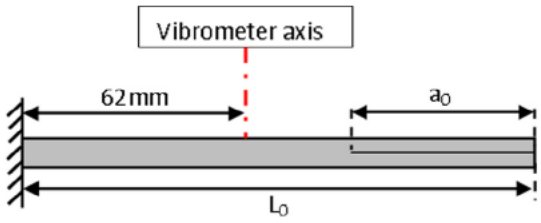

Fig. 10. Test configuration of the specimen (L_0 152 mm for 260 Hz, L_0 122 mm for 400 Hz).

temperature. Some typical temperature evolution curves are plotted in Fig. 11. The maximal increase of temperature never exceeded +12 °C and was obtained for the maximum imposed displacement (d_{imp} 1.2 mm) in all of the tests conducted. Thus specimen temperatures remained far away from the glass transition temperature of the resin (close to 160 °C) which makes any change in material property due to self heating very unlikely.

4.2. Test procedure

First a frequency sweep is achieved to find out the 1st bending resonance frequency of the cracked specimen. Then the level of the maximum displacement is fixed for the fatigue test at resonance. The shaker control device regulates the acceleration level in order to perform the fatigue cycling at the chosen displacement. As the delamination propagates the resonance frequency of the specimen slowly decreases with the corresponding increase of compliance. As a matter of fact, the resonance frequency is followed during the test by keeping constant the phase quadrature (φ) between the input acceleration and the beam displacement (cf. [28] for more details). The test is stopped when the resonance frequency reaches the desired frequency (f_f), corresponding to a propagation of 0.5 mm, generally a few Hz below the initial resonance frequency (Fig. 12). Displacement and resonance frequency are monitored during the whole fatigue cycling for subsequent analysis.

4.3. Data reduction and results

The current delamination length (a) and the maximum ERR (G_{max}) are needed all along the test in order to perform data reduction. Thus two relations have to be set up beforehand:

- first the relation between the resonance frequency and the delamination length,
- and then the relation between ERR and the delamination length at an imposed displacement.

To help with this process, a 3D numerical model of the delaminated beam specimen has been developed with the FEM software Samcef®. The elastic properties used for this model are given in Table 1 except for the Flexural modulus which is fixed to 100 GPa. The specimen is modeled with second degree volumic finite elements of 20 nodes. After a convergence study, a meshing of four elements in the thickness direction (5 mm) and one element per millimeter in length and in width of the specimen has been found to be sufficient to reach consistent results. Delamination crack is achieved by duplicating nodes all over the cracked surface.

First, a linear modal analysis is performed to determine the characteristics of the 1st resonance bending mode, i.e. the deformed mode shape and corresponding modal frequency, as a function of delamination length (Fig. 13a). The mode shape is used to correlate the deflection at the test measurement point with the maximum displacement at the end of the beam as a function of the delamination size.

Then a linear static analysis is performed for each delamination length to compute ERRs with the Virtual Crack Extension method available in Samcef®. For this calculation, contact conditions are defined between upper and lower cracked surfaces. And the static loading is defined as the displacement field corresponding to the mode shape of the delaminated beam for a fixed maximal displacement of 5 mm at the end of the beam. The ERR evolution is then plotted as a function of the delamination length. (Fig. 13b).

In order to take account of the actual experimental clamping conditions, bending modulus of each specimen is adjusted to match the experimental resonance frequency of the specimen, with its initial delamination length (a_0), as measured from the frequency sweep ($freq_{sweep}$) (Fig. 10) Eq. (5).).

$$E_{specimen} \quad E_{numerical} \frac{freq^2_{sweep}}{freq^2_{numerical}} \tag{5}$$

where $E_{specimen}$ is the fitted specimen bending modulus, $E_{numerical}$ the bending modulus used in the FE model (reported in the Table 1), $freq_{sweep}$ the resonance frequency of the specimen at the initial delamination length and $freq_{numerical}$ the numerical frequency of the beam.

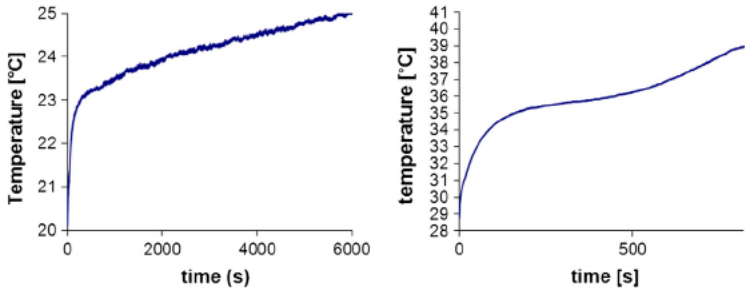

Fig. 11. Time evolution of hot spot temperature during fatigue tests (L_0 122 mm, d_{imp} 1.0 mm on the left and d_{imp} 1.2 mm on the right).

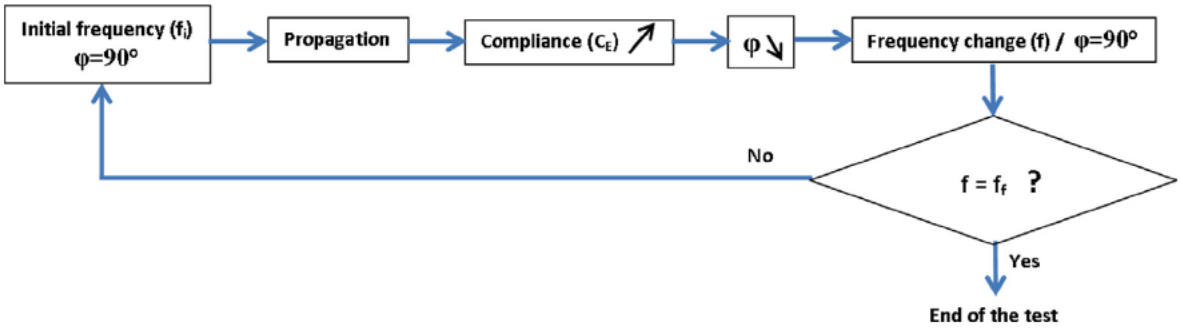

Fig. 12. Test process.

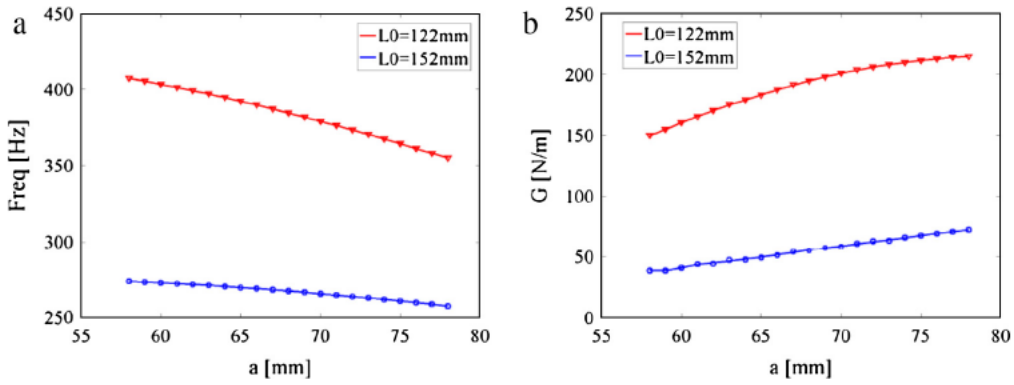

Fig. 13. Numerical simulation results: (a) resonance frequency vs crack length: (b) ERR vs crack length for 5 mm displacement at the beam end (for both free lengths L_o of specimen).

The value of 100 GPa used in the numerical model for the bending modulus was very close to the mean value of 99.6 GPa (standard deviation of 3.6 GPa) obtained for all the specimens. This small difference in modulus was however taken into consideration by redrawing the abacus curves (Fig. 13, Eq. (5)) for each specimen.

Eventually resonance frequency evolution monitored during tests was used to determine the actual crack length with help of the abacus curve of resonance frequency vs delamination length (Fig. 13a). The ERR available for 5 mm displacement at the end of beam was then deduced from the abacus curve ERR vs delamination length (Fig. 13b). The current available ERR for propagation during tests was then determined with the measured displacement during the tests (Eq. (6)).

$$G_{final} \quad G_{numerical} \frac{E_{specimen}}{E_{numerical}} \frac{dep^2_{specimen}}{dep^2_{numerical}} \tag{6}$$

where G_{final} is the test ERR, $G_{numerical}$ the numerical ERR, $dep_{specimen}$ the test displacement of the beam at the measurement point and $dep_{numerical}$ the corresponding numerical displacement.

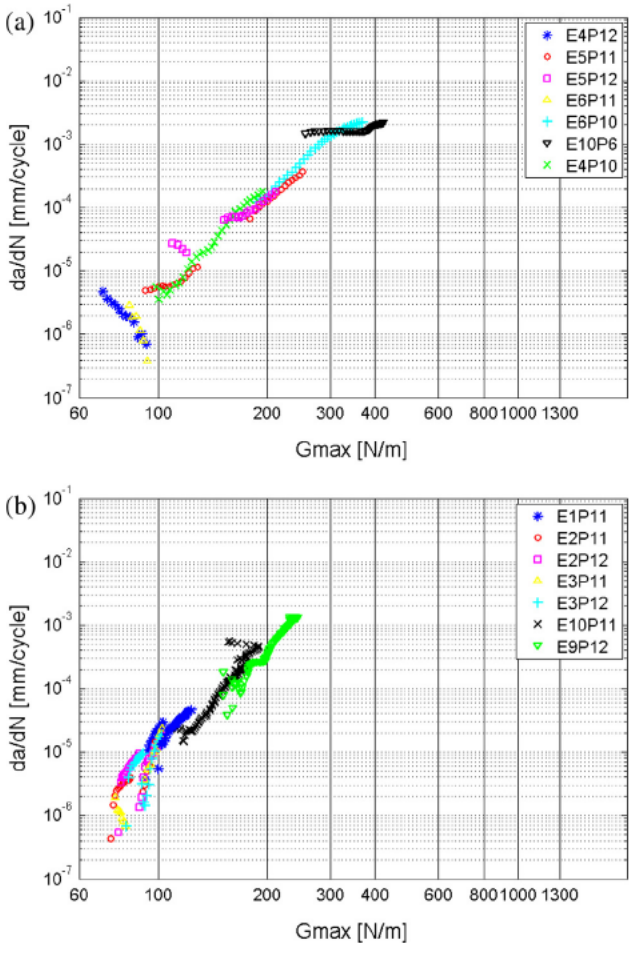

Fig. 14. Propagation rate curve R −1 (260 Hz and 400 Hz from left to right).

Based on the experimental results, it is then possible to plot the evolution of the crack propagation rate as a function of the ERR maximal value at 260 Hz and 400 Hz for the material under study (Fig. 14).

As it was performed for the low frequency tests, a G N onset propagation curve can be extrapolated from the crack propagation rate test results. During the dynamic cycling, the resonance frequency decreases. The Paris law is cut into segments according to a frequency reduction corresponding to a crack extension of 0.5 mm. It is thus possible to plot the following G N onset propagation curves (Fig. 15).

5. Analysis and discussion

5.1. Fatigue crack propagation curves

The results of low frequency tests achieved at $R = 0.1$ and high frequency tests performed at $R =$ 1 are displayed in Fig. 16 where delamination propagation rate is plotted as a function of the normalized G_{max}.

A large discrepancy is clearly observed between high and low frequency results. On one hand results at 400 Hz and 260 Hz both performed at R 1 seem to follow a same linear law. On the other hand low frequency tests performed at 10 Hz and at $R = 0.1$ are roughly two times less critical than tests performed under vibration loading. Around the same factor has already been noticed on results of several authors [11,12,9] between a loading ratio of R 1 and a loading ratio of R 0.1.

The approach developed by Hojo et al. [30] is used to take into account the loading ratio difference. This approach is valid because Paris curve slopes (i.e. the exponent n) are nearly the same for both test conditions.

$$\Delta K_{eq} \quad \Delta K^{1} \ ^{\gamma} K_{max}^{\gamma} \quad \Delta K(1 \quad R) \ ^{\gamma} \tag{7}$$

This relation is then adapted to the use of ERR by defining a ΔG which ensures consistency of this expression with the load ratio and settles similitude between ΔG and ΔK (the Stress Intensity Factor) [9,31]:

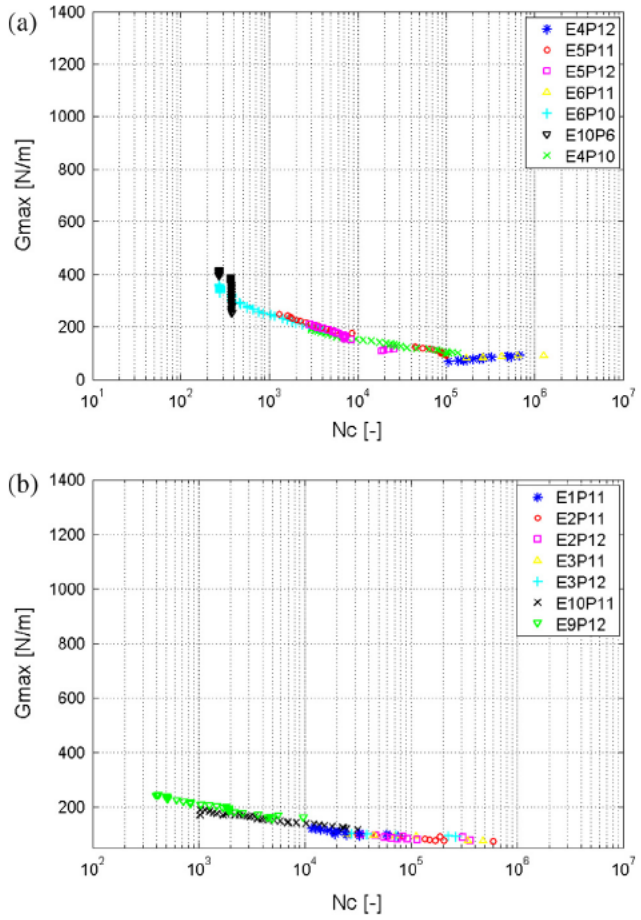

Fig. 15. Dynamical *G–N* onset propagation curve $R \quad -1$ (260 Hz and 400 Hz from left to right).

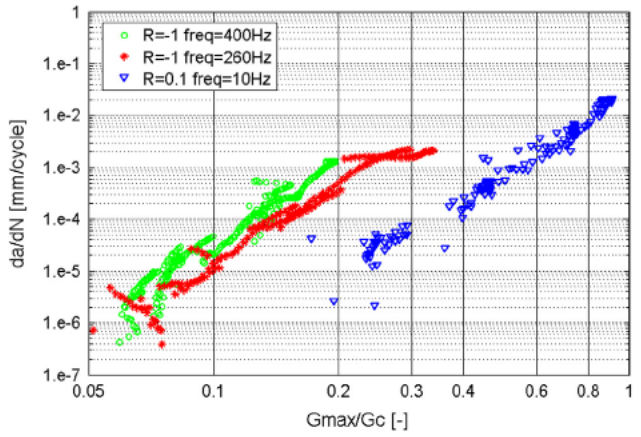

Fig. 16. Propagation rate normalized curve for the frequencies: 10 Hz, 260 Hz and 400 Hz.

$$\Delta G \quad \left(\sqrt{G_{max}} \quad \sqrt{G_{min}}\right)^2 \quad G_{max}(1 \quad R)^2 \tag{8}$$

Using relation (7) it becomes:

$$\Delta G_{eq} \quad \Delta G^{1\ \gamma} G_{max}^{\gamma} \quad \Delta G(1 \quad R)^{\ 2\gamma} \tag{9}$$

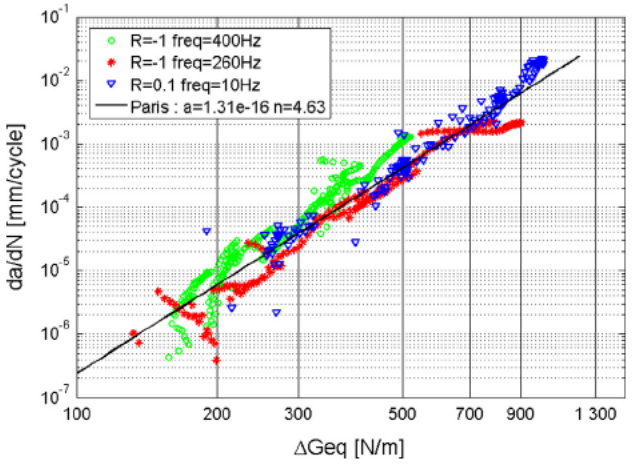

Fig. 17. Propagation rate curve vs ΔG_{eq} for the frequencies: 10 Hz, 260 Hz and 400 Hz.

A value of 0.45 for γ is identified by fitting test results. Crack propagation rate is then plotted as a function of ΔG_{eq} for each test condition. Results follow a global mean Paris curve (Fig. 17):

$$\frac{da}{dN} \quad k_D \cdot \Delta G_{eq}^{n_D} \tag{10}$$

This value of 0.45 is consistent with the difference in loading ratio results between R 0.1 and R 1 mentioned before.

At low propagation rate it seems that there is a non propagation threshold associated with a large scattering of data from the interpolated linear curve.

A main ΔG_{eq} N onset propagation curve can be plotted by using crack propagation rate data as before (Eq. (11), Fig. 18)).

$$\Delta G_{eq} \quad p_D \cdot N_c^{m_D} \tag{11}$$

It can be observed in the above figure (Fig. 18)) that the identified ΔG_{eq} N onset propagation curve should intersect the vertical axis for a value larger than 1000 N/m which seems consistent with the experimental static critical ERR value of 1240 N/m. The non propagation fatigue threshold ERR value seems to be lower than ΔG_{eq} 200 N/m.

5.2. Fracture surface observations

Micrographs obtained by Scanning Electron Microscopy show that fracture surfaces are dominated by shear cusps (or scallops), as it is expected for mode II crack surfaces. However, depths and widths of the cusps seem to be influenced by the loading level (Fig. 19). Furthermore the lower the frequency, the deeper and wider the cusps are. Fracture surfaces also

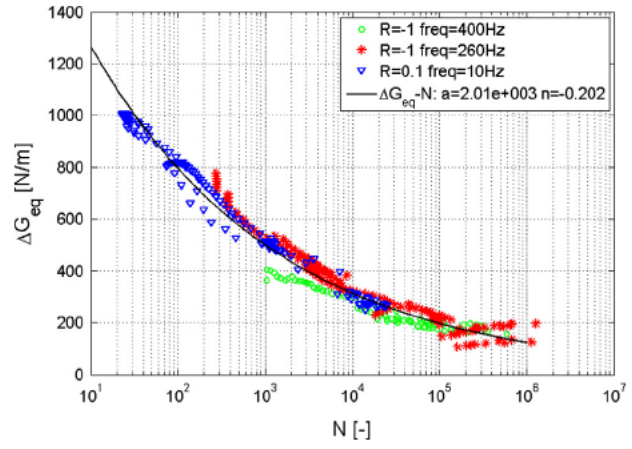

Fig. 18. ΔG_{eq}–N curve for the frequencies: 10 Hz, 260 Hz and 400 Hz. (a) ΔG_{eq} around 350 N/m at 260 Hz. (b) ΔG_{eq} around 500 N/m at 260 Hz.

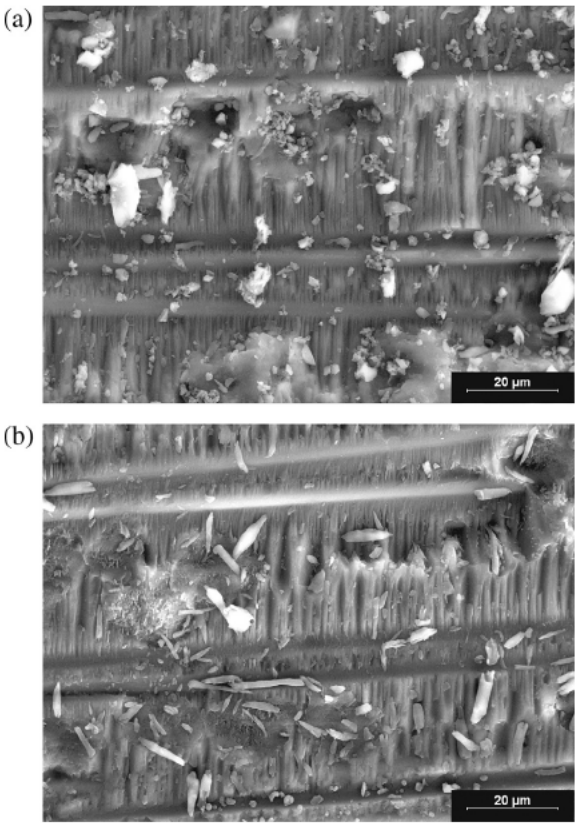

Fig. 19. Scallops size. (a) 10 Hz. (b) 260 Hz.

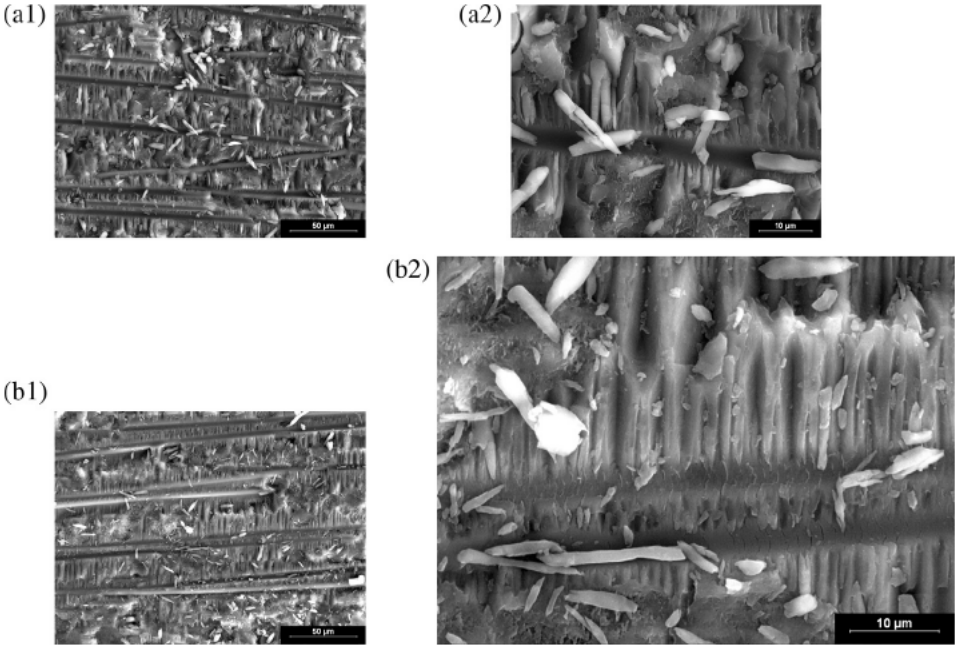

Fig. 20. Micrographs for ΔG_{eq} around 500 N/m.

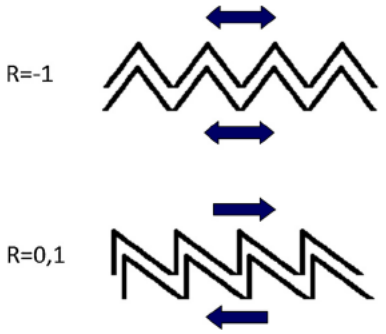

Fig. 21. Scallops shape and loading ratio.

show matrix rollers which are rounded pieces of matrix material as already identified by Sjogren et al. [27] for mode II fatigue delamination.

Comparison of micrographs at 10 Hz and 260 Hz for the same ΔG_{eq} level reveals noticeable differences in the scallops feature (Fig. 20). This is likely due to an effect of the loading ratio as already observed by Matsubara et al. [9]. The loading at R 1 is symmetrical and allows a symmetrical matrix damage which results in isosceles triangular shapes. At R 0.1, the shear loading is always in the same direction, and cusps take shape of rectangular triangles (Fig. 21). Furthermore scallops present squashed tips for tests at R 1 and 260 Hz while at R 0.1 and 10 Hz tips are sharper.

5.3. Frequency effects

As proposed in the Fatigue crack propagation curves section, it is possible to gather fatigue crack propagation curves obtained for different frequencies into a single master curve characterizing the fatigue crack propagation behavior of the T700 M21 material. This should be very helpful in order to design a structure under the damage tolerance approach.

Several comments should support the idea of a limited frequency influence in these experimental results:

- For the investigated frequency range [10 400 Hz], the creep effect is very likely to be limited at room temperature.
- Imposed displacements for fatigue loadings are fixed at sufficiently low levels to avoid any detrimental self heating effect (Part Test configuration).
- Loading rate has very likely no identified effect on mode II delamination propagation in fatigue as mentioned in the review of Cantwell et al. [32].

However we must be very cautious in trying to generalize this conclusion. Indeed it is observed in Fig. 14 at 260 Hz that at low ERR values, around 7% of the critical static ERR, crack propagation rate decreases noticeably with increasing ERR. This is also observed for the 400 Hz case to a much lesser extent. This effect calls for further investigations.

6. Conclusions

A specific dynamic test has been set up to perform Fatigue Crack Propagation Rate test at high frequency for unidirectional composite laminates under mode II. Delaminated specimens are loaded at their 1st bending mode resonance frequency. Imposed displacements are low enough to limit any self heating during fatigue loading. Natural frequency evo lution as a function of crack length is used to control the fatigue test. A data reduction process, which partly uses numerical simulations, has been developed to analyse the results.

Mode II fatigue tests have then been achieved at different frequencies to investigate the fatigue crack propagation behavior of the T700/M21 composite material. First classical ENF tests have been conducted at 10 Hz. Crack Propagation Rate vs maximal Energy Restitution Rates follows a linear law for this material. G N onset propagation curves have been extrap olated from the test data since the material behavior seems to be neither influenced by loading history nor influenced by propagation history.

Fatigue resonance results obtained for both dynamic tests at 260 Hz and 400 Hz feature the same evolution when Crack Propagation Rate (CPR) is plotted as a function of G_{max}. This indicates no effect or at least minor effect of frequency in this range of frequency for the material under study. On the contrary, large differences are noticed between the two types of tests when plotted vs G_{max}. It seems that it can be attributed to the loading ratio difference between ENF and ELS tests. With a convenient data reduction and definition of ΔG_{eq}, CPR results at all frequencies plotted vs ΔG_{eq} follow the same quasi linear curve. A no propagation threshold fatigue value seems likely to be lower than ΔG_{eq} of 200 N/m.

In this test configuration the T700/M21 material seems to be insensitive to high frequency effects. Delamination propa gation behavior of carbon fiber epoxy resin composites of such type might be determined with high frequency tests. If so,

dynamical fatigue at resonance should largely accelerate test durations. However, further tests have to be completed and performed for other load ratios and other materials in order to support this eventuality.

References

[1] Dhainaut JM, Guo XY, Mei C, Spottswood SM, Wolfe HF. Nonlinear random response of panels in an elevated thermal-acoustic environment. J Aircraft 2003;40(4):683–91.
[2] Kouchakzadeh MA, Rasekh M, Haddadpour H. Panel flutter analysis of general laminated composite plates. Compos Struct 2010;92(12):2906–15.
[3] AMC-2010. Proof of structure – fatigue and damage tolerance in AMC 20-29 composite aircraft structure; 2010.
[4] Hojo M, Ando T, Tanaka M, Adachi T, Ochiai S, Endo Y. Mode I and II interlaminar fracture toughness and fatigue delamination of CF/epoxy laminates with self-same epoxy interleaf. Int J Fatigue 2006;28(10):1154–65.
[5] Peng L, Zhang J, Zhao L, Bao R, Yang H, Fei B. Mode I delamination growth of multidirectional composite laminates under fatigue loading. J Compos Mater 2010;45(10):1077–90.
[6] Brunner AJ, Stelzer S, Pinter G, Terrasi GP. Mode II fatigue delamination resistance of advanced fiber-reinforced polymer-matrix laminates: towards the development of a standardized test procedure. Int J Fatigue 2013;50:57–62.
[7] ASTM-D6115. Standard test method for mode I fatigue delamination growth onset of unidirectional fiber-reinforced polymer matrix composite; 1987.
[8] Blackman BRK, Brunner AJ, Williams JG. Mode II fracture testing of composites: a new look at an old problem. Engng Fract Mech 2006;73(16):2443–55.
[9] Matsubara G, Ono H, Tanaka K. Mode II fatigue crack growth of delamination in unidirectional tape and satin-woven fabrics laminates of high strength GFRP. Int J Fatigue 2006;28(10):1177–86.
[10] Nakai Y, Hiwa C. Effects of loading frequency and environment on delamination fatigue crack growth of CFRP. Int J Fatigue 2002;24:161–70.
[11] Russell AJ, Street KN. The effect of matrix toughness on delamination: static and fatigue fracture under mode II shear loading of graphite fiber composites. Tough Compos, ASTM STP 1987;937:275–94.
[12] Tanaka K, Tanaka H. Stress-ratio effect on mode II propagation of interlaminar fatigue cracks in graphite/epoxy composites. ASTM Special Tech Publ 1997;1285:126–42.
[13] Herztberg RW, Manson JA. Fatigue of engineering plastics. Academic Press; 1980.
[14] Xiao XR. Modeling of load frequency effect on fatigue life of thermoplastic composites. J Compos Mater 1999;33(12):1141–58.
[15] Hahn HT, Turkgenc O. The effect of loading parameters on fatigue of composite laminates: part IV information systems. Technical report, DOT/FAA/AR-00/48; 2000.
[16] Rotem A. Load frequency effect on the fatigue strength of isotropic laminates. Compos Sci Technol 1993;46(2):129–38.
[17] Barron V, Buggy M, McKenna NH. Frequency effects on the fatigue behaviour on carbon fibre reinforced polymer laminates. J Mater Sci 2001;36 (7):1755–61.
[18] Kharrazi MR, Sarkari S. Frequency-dependent fatigue damage accumulation in fiber-reinforced plastics. J Compos Mater 2001;35(21):1924–53.
[19] Minak G. On the determination of the fatigue life of laminated graphite–epoxy composite by means of temperature measurement. J Compos Mater 2010;44(14):1739–52.
[20] Rotem A. Effect of the frequency of the alternating load on fatigue delamination of laminates. SAMPE J 1994;30(3):10–6.
[21] Michel SA, Kieselbach R, Martens HJ. Fatigue strength of carbon fibre composites up to the gigacycle regime (gygacycle-composites). Int J Fatigue 2006;28(3):261–70.
[22] Wang QY, Sriraman MR, Kawagoshi N, Chen Q. Fatigue crack growth of bonded composite repairs in gigacycle regime. Int J Fatigue 2006:1197–201.
[23] Hosoi A, Sato N, Kusumoto Y, Fujiwari K, Kawada H. High-cycle fatigue characteristics of quasi-isotropic CFRP laminates over 10^8 cycles (initiation and propagation of delamination considering interaction with transverse cracks). Int J Fatigue 2010;32:29–36.
[24] Ramsteiner F, Armbrust T. Fatigue crack growth in polymers. Polym Test 2001;20:321–7.
[25] Yuen BKC, Taheri F. The effects of loading frequency, tensile overload and compressive underload on the fatigue crack propagation behaviour of polymethyl methacrylate. Polym Test 2004;23:491–500.
[26] Merah N, Saghir F, Khan Z, Bazoune A. Modeling the combined effects of temperature and frequency on fatigue crack growth of chlorinated polyvinyl chloride (CPCV). Engng Fract Mech 2005;72(11):1691–701.
[27] Sjogren A, Asp LE. Effects of temperature on delamination growth in a carbon/epoxy composite under fatigue loading. Int J Fatigue 2002;24(2–4):179–84.
[28] Maillet I, Michel L, Rico G, Fressinet M, Gourinat Y. A new test methodology based on structural resonance for mode I fatigue delamination growth in unidirectional composite. Compos Struct 2013;97:353–62.
[29] Saravanos DA, Hopkins DA. Effects of delaminations on the damped dynamic characteristics of composite laminates: analysis and experiments. J Sound Vib 1996;192(5):977–93.
[30] Hojo M, Tanaka K, Gustafson CG, Hayashi R. Effect of stress ratio on near-threshold propagation of delamination fatigue cracks in unidirectional CFRP. Compos Sci Technol 1987;29(4):273–92.
[31] Rans C, Alderliesten R, Benedictus R. Misinterpreting the results: how similitude can improve our understanding of fatigue delamination growth. Compos Sci Technol 2011;71:230–8.
[32] Cantwell WJ, Blyton M. Influence of loading rate on the interlaminar fracture properties of high performance composites – a review. Appl Mech Rev 1999;52(6):199–212.